SCIENTIFIC REPORTS

OPEN

The effects of oxygen in spinel oxide $Li_{1+x}Ti_{2-x}O_{4-\delta}$ thin films

Yanli Jia[1,2], Ge He[1,2], Wei Hu[1,2], Hua Yang[1,2], Zhenzhong Yang[1,2], Heshan Yu[1,2], Qinghua Zhang[1,2], Jinan Shi[1,2], Zefeng Lin[1,2], Jie Yuan[1,2], Beiyi Zhu[1,2], Lin Gu[1,2,3], Hong Li[1,2,3] & Kui Jin[1,2,3]

Received: 23 August 2017
Accepted: 25 January 2018
Published online: 05 March 2018

The evolution from superconducting $LiTi_2O_{4-\delta}$ to insulating $Li_4Ti_5O_{12}$ thin films has been studied by precisely tuning the oxygen pressure in the sample fabrication process. In superconducting $LiTi_2O_{4-\delta}$ films, with the increase of oxygen pressure, the oxygen vacancies are filled gradually and the *c*-axis lattice constant decreases. When the oxygen pressure increases to a certain critical value, the *c*-axis lattice constant becomes stable, which implies that the sample has been completely converted to $Li_4Ti_5O_{12}$ phase. The two processes can be manifested by the angular bright-field images of the scanning transmission electron microscopy techniques. The transition temperature (T_{ch}) of magnetoresistance from the positive to the negative shows a nonmonotonic behavior, *i.e.* first decrease and then increase, with the increase of oxygen pressure. We suggest that the decrease T_{ch} can be attributed to the suppressing of orbital-related state, and the inhomogeneous phase separated regions contribute positive MR and thereby lead to the reverse relation between T_{ch} and oxygen pressure.

In the research on oxide superconductors, the oxygen always plays an important role in the superconductivity and their normal state behaviors[1,2]. In copper oxide high- critical temperature (T_c) superconductors, such as $Nd_{2-x}Ce_xCuO_{4\pm\delta}$[3–5], $Pr_{2-x}Ce_xCuO_{4\pm\delta}$[6–8] and $YBa_2Cu_3O_{7-\delta}$[9–11], T_c can be greatly improved in a large range by adjusting the oxygen content during the annealing process, as well as the titanium oxide systems, such as $SrTiO_3$[12,13] and TiO[14,15]. Oxygen has a strong effect not only on superconductivity, but also on many other properties. For instance, the antiferromagnetism[16] and the charge density wave[17] can also be tuned by the oxygen vacancies. Furthermore, the doping and disorder effects induced by oxygen vacancies can cause obviously change on Hall resistance and magnetoresistance (MR) behaviors in the normal state[5,6,18]. Studying the oxygen effects is of great help to understand the mechanism of superconductivity, transport and other properties of the oxide superconductor[9,19,20].

Among hundreds of spinel oxides, the metallic lithium titanate $LiTi_2O_4$ is the only known oxide superconductor, which T_c is as high as 13.7 K[21], discovered by Johnston *et al.* in 1973[22]. Previous studies have disclosed that $LiTi_2O_4$ is a BCS *s*-wave superconductor with intermediate electron-phonon coupling ($\lambda_{el\text{-}ph} \sim 0.65$)[23,24]. Nevertheless, an enhanced density of states has been unveiled by magnetic susceptibility[25] and specific heat measurements[23], indicating that *d-d* electronic correlations cannot be ignored in this system. Meanwhile, due to the mixed-valence of Ti ions in the frustrated Ti sublattice, $LiTi_2O_4$ exhibits complicated spin-orbit fluctuations, which is evidenced by the resonant inelastic soft-x-ray scattering[26], nuclear magnetic resonance[27] and magnetic susceptibility measurements[25]. Very recently, electrical transport and tunneling spectra measurements on high quality epitaxial [001]-oriented $LiTi_2O_4$ films have revealed an orbital-related state below ~50 K, confirmed by a twofold in-plane angular dependent MR, positive MR as well as the relation $\Delta \sim -B^2$ [28].

Interestingly, by tuning the oxygen in the process of sample deposition, the phase of the thin film changes from $LiTi_2O_{4-\delta}$ to $Li_4Ti_5O_{12}$ along with the superconductor-insulator phase transition[29]. However, this transition seems to happen abruptly, which hinders us from understanding the nature of the transition. Previous work on $LiTi_2O_4$ polycrystals has disclosed that the existence of oxygen-site distortion induces prominent changes in the electronic states near E_F[30]. In addition, tunneling spectra experiments on $LiTi_2O_4$ films of different orientations reveal an anisotropic electron-phonon coupling in this system, which is regarded to originate from the *Jahn-Teller* distortions enhanced by oxygen vacancies[31]. Nevertheless, it is still unclear what happens in the microstructure of the sample during the transition from $LiTi_2O_4$ to $Li_4Ti_5O_{12}$. Moreover, the mechanism of the oxygen effects on superconductivity of

[1]Beijing National Laboratory for Condensed Matter Physics, Institute of Physics, Chinese Academy of Sciences, Beijing, 100190, China. [2]School of Physical Sciences, University of Chinese Academy of Sciences, Beijing, 100049, China. [3]Collaborative Innovation Center of Quantum Matter, Beijing, 100190, China. Yanli Jia and Ge He contributed equally to this work. Correspondence and requests for materials should be addressed to K.J. (email: kuijin@iphy.ac.cn)

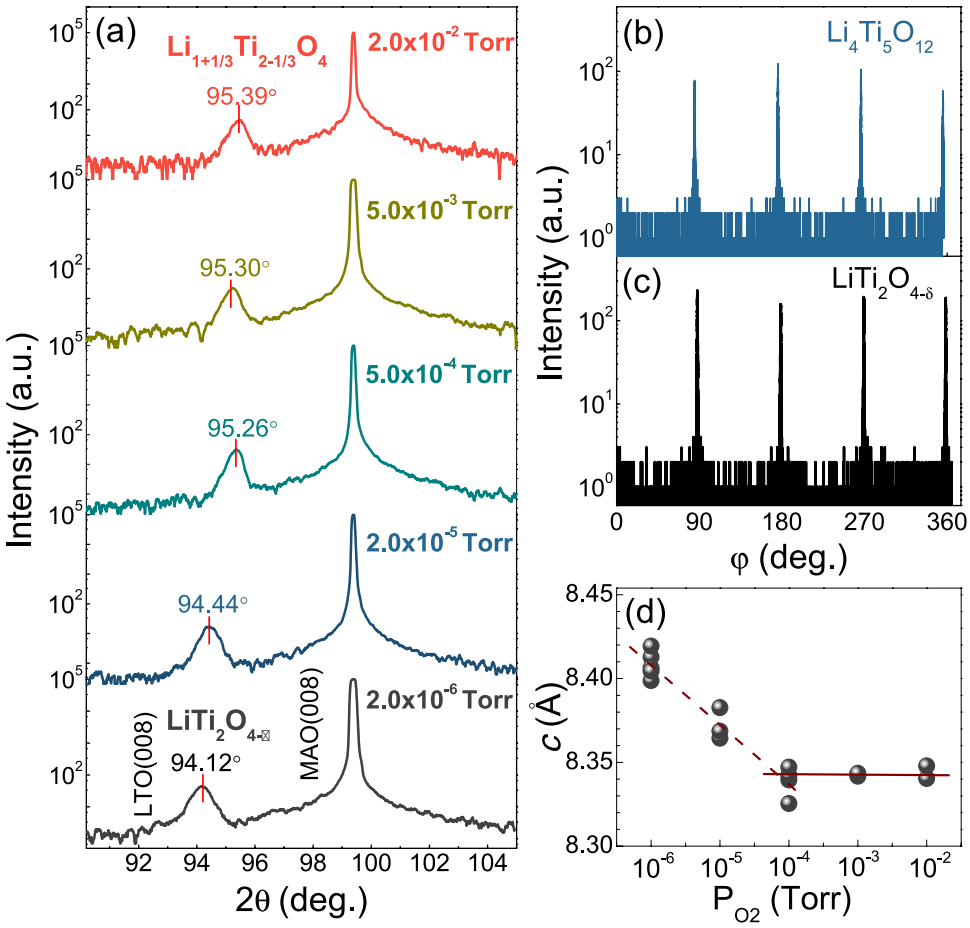

Figure 1. (**a**) The θ–2θ XRD spectra of epitaxial $Li_{1+x}Ti_{2-x}O_{4-\delta}$ ($0 \leq \times \leq 1/3$) thin films grown on (001) MAO substrates at different P_{O2}. (**b**) The φ-scan measurements of $LiTi_2O_{4-\delta}$ and $Li_4Ti_5O_{12}$ thin films on MAO (001) in the (404) reflection. (**c**) The lattice constant along *c* axis of the samples versus P_{O2}.

$LiTi_2O_4$ has never been investigated, as well as the transport behaviors in the normal state. Therefore, it is worthy of tuning the oxygen pressure (P_{O2}) in the process of film deposition to clarify these questions.

In this work, we carefully manipulated the transition from $LiTi_2O_{4-\delta}$ to $Li_4Ti_5O_{12}$ thin films by adjusting the P_{O2} in the process of pulsed laser deposition (PLD). First, the high quality $LiTi_2O_{4-\delta}$ superconducting thin films can be obtained in the high vacuum environment. Tuning the P_{O2} from 10^{-7} to 10^{-4} Torr, the *c*-axis lattice constant gradually decreases, indicating that the filling of oxygen vacancies dominates in this process. Second, when P_{O2} is higher than 10^{-4} Torr, the *c*-axis lattice constant stops to decrease, indicating the finish of transition from $LiTi_2O_{4-\delta}$ to $Li_4Ti_5O_{12}$ phase. These two processes can be revealed from the angular bright-field images (ABF) of $LiTi_2O_{4-\delta}$ and $Li_4Ti_5O_{12}$ by the scanning transmission electron microscopy (STEM) techniques. In addition, the temperature (T_{ch}) of MR from the positive to the negative shows a nonmonotonic behavior, *i.e.* first decrease and then increase, with the increase of P_{O2}. Combined with the electron energy-loss spectroscopy (EELS) measurements, we suggest that the decrease of T_{ch} under lower P_{O2} stems from the suppression of orbital-related state via filling the oxygen vacancies, and the increase of T_{ch} under higher P_{O2} is due to the phase separation in some regions, which dominates the positive MR (p-MR).

Results and Discussion

The θ–2θ XRD spectra of (001) $Li_{1+x}Ti_{2-x}O_{4-\delta}$ ($0 \leq \times \leq 1/3$) samples grown in different P_{O2} are shown in Fig. 1(a). The (001)-oriented $LiTi_2O_{4-\delta}$ thin films are achieved when the films are deposited under $P_{O2} \leq 10^{-6}$ Torr. Instead, the (001)-oriented $Li_4Ti_5O_{12}$ thin films are formed at $P_{O2} > 10^{-4}$ Torr. The XRD patterns of the samples in different P_{O2} are quite similar except that the diffraction peaks gradually shift to higher angle in the $LiTi_2O_{4-\delta}$ films at larger P_{O2}. In order to check the crystallization quality of the thin films, we also perform φ-scan. In Fig. 1(b), the φ-scans of (404) plane of both $LiTi_2O_{4-\delta}$ and $Li_4Ti_5O_{12}$ samples display four-fold symmetry with uniformly distributed peaks. From the θ–2θ XRD spectra, we can extract the value of the out-of-plane lattice constant (*c-axis*) as a function of the P_{O2}. As seen in Fig. 1(c), when $P_{O2} < 10^{-4}$ Torr, *c* gradually decreases with increasing P_{O2}. However, when P_{O2} is higher than 10^{-4} Torr, *c* is saturated, indicating the complete formation of $Li_4Ti_5O_{12}$ phase. As a result, a phase transition from $LiTi_2O_{4-\delta}$ to $Li_4Ti_5O_{12}$ has been successfully achieved by tuning P_{O2} during the sample deposition.

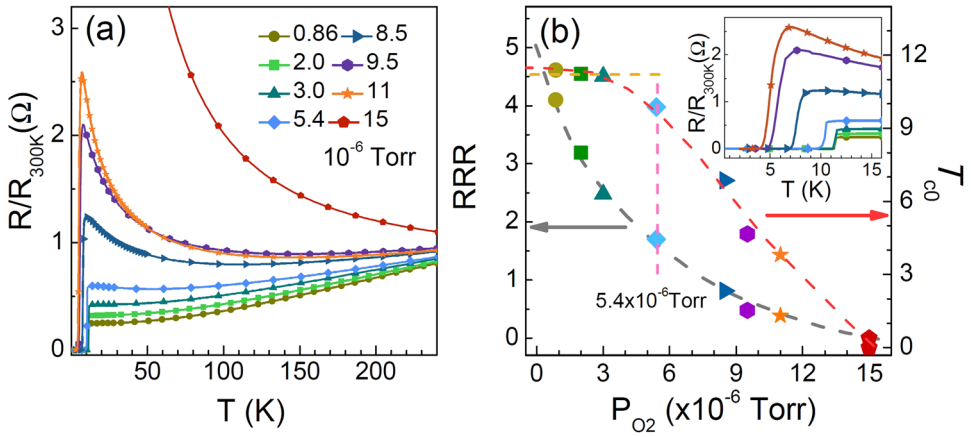

Figure 2. (**a**) The *R*-*T* curves of $Li_{1+x}Ti_{2-x}O_{4-\delta}$ ($0 \leq \times \leq 1/3$) thin films grown on (001) MAO substrate with different P_{O2} during the deposition. (**b**) The P_{O2} dependence of *RRR* and T_{c0} of the films in (**a**) are plotted. The gray and red dashed lines are used to guide eyes. T_{c0} is defined as the temperature where resistance is lower than 10^{-6} Ohm. Inset: zoom the *R*-*T* curves in Fig. 2(a) at low temperature range.

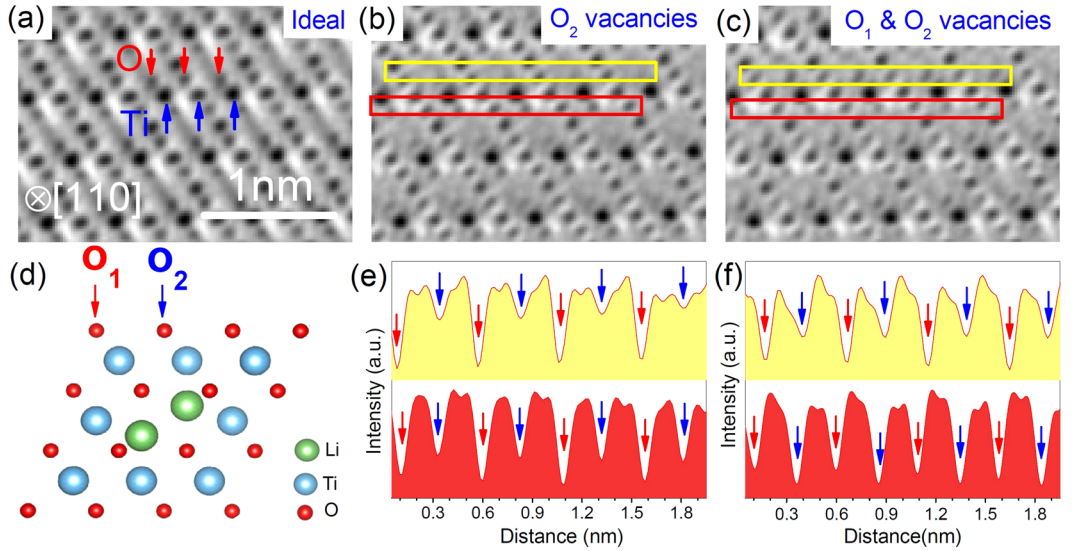

Figure 3. ABF images of $LiTi_2O_{4-\delta}$ thin film in (**a**) pristine, (**b**) O_2 vacancy and (**c**) O_1 & O_2 vacancy regions. (**d**) Structure model of $LiTi_2O_4$ projected along [110] direction, where the atomic positions of both O_1 and O_2 oxygen are labeled by red and blue arrow, respectively. (**e**) and (**f**) Line profiles of ABF contrast with filled yellow and red color, obtained from the corresponding yellow and red areas in (**b**) and (**c**), respectively. Atomic positions of O_1 and O_2 are also labeled by red and blue arrows, respectively. Note that the lower panel in (**e**) exhibits contrast between O_1 (red arrows) and O_2 (blue arrows) close to the ideal structure.

In order to further study the effects of oxygen on superconducting state and normal state, we systematically measured the resistances of various thin films from $LiTi_2O_{4-\delta}$ to $Li_4Ti_5O_{12}$. The R-T curves of the $LiTi_2O_{4-\delta}$ thin films with different oxygen pressures are shown in Fig. 2(a). Increasing the P_{O2} during the deposition, the samples undergo a transition from metal to insulator in the normal state. In Fig. 2(b), the residual resistivity ratio (*RRR*) decreases monotonically with increasing P_{O2}. Here, the *RRR* is defined as the ratio of room temperature resistivity to the resistivity of T_c^{onset}, *i.e.* $R\,(300\,K)/R\,(T_c^{onset})$, where the T_c^{onset} is the critical temperature at the beginning of superconducting transition. We plot the dependence of T_{c0} on P_{O2} as seen in Fig. 2(b), and the T_{c0} of the $LiTi_2O_{4-\delta}$ thin films is quite stable at $P_{O2} < 5.4 \times 10^{-6}$ Torr, whereas it drops rapidly when $P_{O2} > 5.4 \times 10^{-6}$ Torr.

To find out the microstructure evolution from $LiTi_2O_{4-\delta}$ to $Li_4Ti_5O_{12}$, we have carried out atomic-resolution STEM measurements on these high-quality samples. Figure 3 shows the ABF images along the [110] direction and the corresponding line profiles in different regions with different types of oxygen vacancies. In Fig. 3(a), the O columns, as indicated by red arrows, are imaged as dark spots due to the absorption nature of the ABF contrast, and the contrast of the Ti columns as indicated by the blue arrows is darker than the O columns based on the $\sim Z^{1/3}$ contrast mechanism where Z is the atomic number. Thus, in the pristine regions the contrast of O_1 and O_2 is of

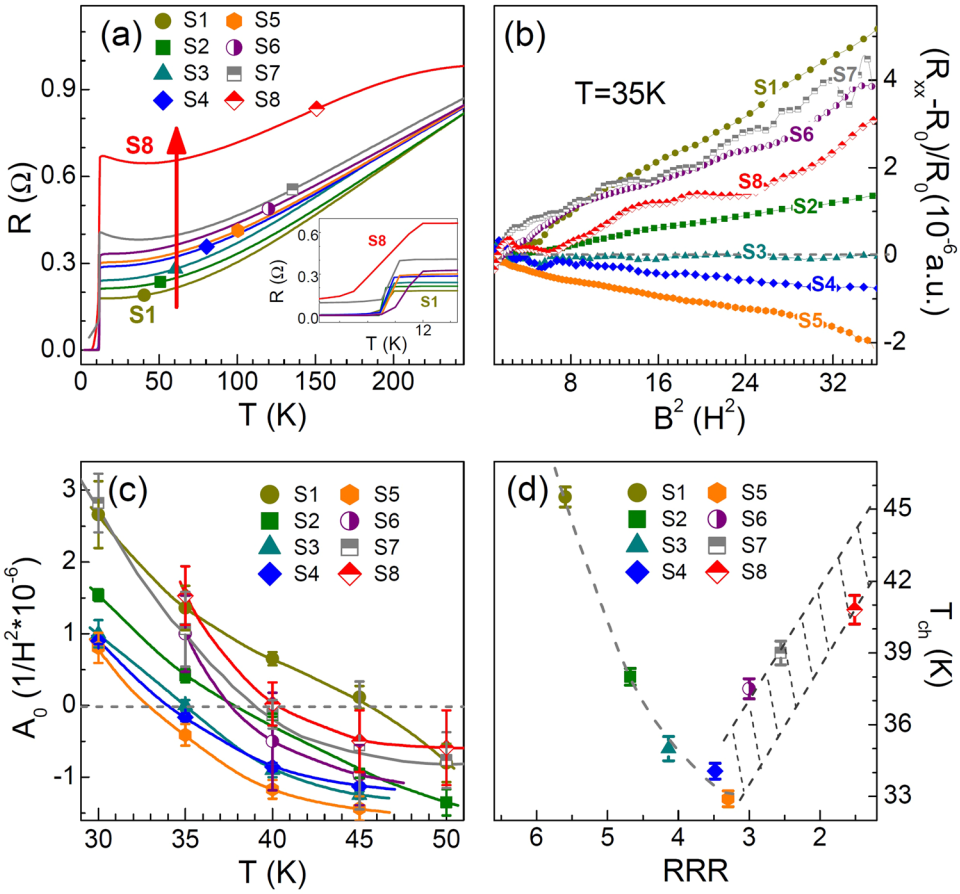

Figure 4. (**a**) The *R*-T curves with increase of P_{O2} are defined as S1–S8 in sequence. The inset is the zoom of *R*-T curves. (**b**) The field dependence of MR of S1–S8 grown on (001) MAO substrates at 35 K. (**c**) The slope value A_0 of MR can be obtained for various samples at different temperatures. With temperature increasing, the value of A_0 changes from the positive to the negative. (**d**) The relationship between *RRR* and T_{ch}. The gray dashed line is used to guide eyes. The shadow areas represent the uncertainties in defining T_{ch} due to the impurities.

approximate equal darkness, and oxygen vacancies as shown in Fig. 3(b) and (c), are imaged as light gray spots. Here, we divided the positions of oxygen atoms into two types, *i.e.* O_1 and O_2 (see Fig. 3(d)) to describe clearly the distribution of oxygen vacancies, as shown by the red and blue arrows. To visualize the oxygen vacancies clearly, we extracted the line profiles on the oxygen rows as indicated by the yellow and red rectangles.

From the line profile of ABF contrast in Fig. 3(e), we can find that the depth of the ABF contrast valley (darkness) at O_2 positions is lower than that at O_1 as seen in the [110] direction, which means some vacancies exist in the O_2 sites. Similarly, some vacancies at O_1 and O_2 exist in another region as shown in Fig. 3(f). However, these oxygen vacancies have not been observed in the $Li_4Ti_5O_{12}$ samples[32]. It is known that the $LiTi_2O_{4-\delta}$ exhibits serious aging effects in forms of polycrystal and single crystal[30]. The $LiTi_2O_{4-\delta}$ thin films, especially the one deposited in the higher vacuum, are much more stable. It is reasonable to speculate that the samples in higher vacuum will contain more oxygen vacancies. Increasing oxygen pressure will fill these oxygen vacancies and finally turn the superconducting phase to insulating $Li_4Ti_5O_{12}$.

The phase evolution with P_{O2} should inevitably make difference in the electronic states. In $LiTi_2O_{4-\delta}$, one concern is about the orbital-related state. Normally, the formation of the orbital order results from the band split near the Fermi level. As for $LiTi_2O_{4-\delta}$, the distortion of Ti-O octahedron leads the splitting of Ti 3d band to e_g and t_{2g} band[33], and the orbital-related state is expected to exist. Although it has been unveiled in previous work, it remains unclear in the origin[25]. One of the evidence is the crossover from the negative MR (n-MR) to the p-MR at $T_{ch} \sim 50$ K in the normal state. Entering the superconducting state, the orbital-related state interacts with Cooper pairs and results in an unexpected relation between the superconducting gap and the applied magnetic field, *i.e.* $\Delta \sim -B^2$. This relation implies the coexistence of the superconducting state and the orbital-related state. Therefore, it is deserved to clarify how the oxygen makes the influence on these two states.

To clarify this issue, we finely tune the P_{O2} around 10^{-6} Torr to avoid the $Li_4Ti_5O_{12}$ phase. Then, we focus on the effects of P_{O2} on R and MR. In the precise tuning process, the vacuum value is not a good scale due to the limitation of the vacuum gauge. Fortunately, the *RRR* decreases monotonically with the increase of oxygen pressure, which can reflect the trend of P_{O2} and the oxygen defects as discussed above. Thus, we use *RRR* to index the samples, named S1 to S8 with *RRR* in the range between 5.6 and 1.5. As shown in Fig. 4(a), the T_c seems unchanged

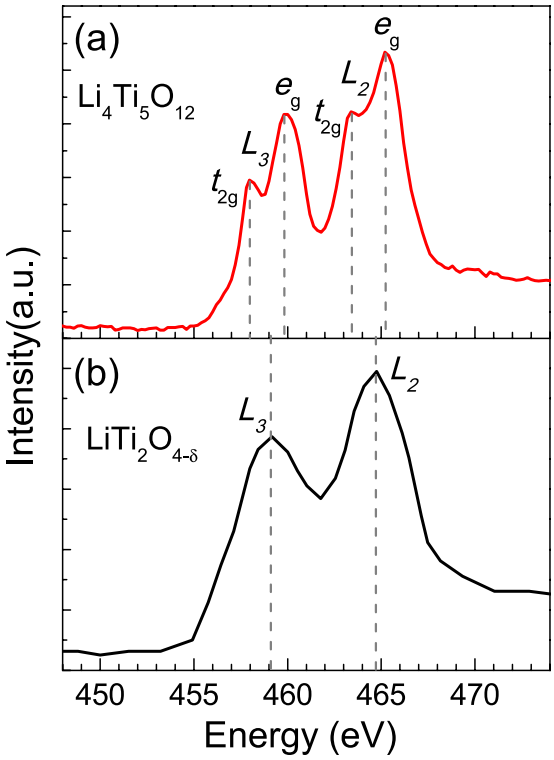

Figure 5. (**a**) The EELS profiles for Ti $L_{2,3}$ edges of the $Li_4Ti_5O_{12}$ thin film. The L_2 and L_3 edges split into four peaks. (**b**) The EELS profiles for Ti $L_{2,3}$ edges of the $LiTi_2O_{4-\delta}$ thin film. Only two peaks appear of $L_{2,3}$ edges.

in the tuning range. For samples S1 to S5, the MR at 35 K changes from positive to negative as seen in Fig. 4(b). By fitting the MR with the Kohler's formula, *i.e.* MR ~A_0B^2[2], the slope A_0 can be obtained for these samples at different temperatures. In Drude model, A_0 is proportional to μ^2 (*i.e.* $\mu = e\tau/m$) with μ the mobility, τ the relaxation time and m the electron mass. With the increase of temperature, the value of A_0 decreases from positive to negative as seen in Fig. 4(c). A negative mobility cannot be understood in this simplified model, and the n-MR is interpreted as the suppression of spin-orbital fluctuations in this system[28]. The T_{ch} from p-MR to n-MR is extracted from Fig. 4(c) and plotted in Fig. 4(d). From S5 to S1, T_{ch} gradually increases with the increase of *RRR*.

However, further reducing the *RRR*, the relation between T_{ch} and *RRR* will be broken. For instance, the MR becomes stronger for the samples deposited under higher P_{O2}, *e.g.* S6–S8, and thus the T_{ch} goes up. In this regime, the formation of $Li_4Ti_5O_{12}$ phase may lead to more boundaries in phase separated samples. Such inhomogeneity in the magnetic field usually exhibits strong p-MR[34,35]. For the samples S1–S5, the p-MR below T_{ch} mainly origins from the orbital-related state since the $LiTi_2O_{4-\delta}$ phase dominates the transport[25]. We speculate that filling the oxygen vacancies seems to suppress the p-MR but in fact the orbital-related state.

In order to verify this assumption, we should evaluate the effects of oxygen vacancies on Ti valance. Although oxygen vacancies have been detected by STEM, the content of oxygen vacancies cannot be quantified. Therefore, we collected EELS profiles of both $LiTi_2O_{4-\delta}$ and $Li_4Ti_5O_{12}$ films. As seen in Fig. 5, the Ti $L_{2,3}$ edges, from $2p_{1/2}$ and $2p_{3/2}$ to $3d$ orbits respectively, split into two peaks in $Li_4Ti_5O_{12}$, but not in $LiTi_2O_{4-\delta}$. Usually, the splitting of $L_{2,3}$ is attributed to the degeneracy lifting of Ti $3d$ orbits by the crystal field.

The missing split of peaks in $LiTi_2O_{4-\delta}$ EELS may origin from two reasons. First, the energy gap between e_g and t_{2g}, named Δ_{e-t}, is too small to be discernable in EELS. According to the band calculations, Δ_{e-t} equals to 2.1 eV and 2.4 eV for the ideal structure $LiTi_2O_4$ and $Li_4Ti_5O_{12}$, respectively[36]. Moreover, four peaks were also observed in $Li_7Ti_5O_{12}$, where Δ_{e-t} equals to 1.8 eV[32]. Considering the existence of oxygen vacancies, which may further distort the Ti-O octahedrons, we do not expect a smaller crystal field. Therefore, the change of Δ_{e-t} cannot account for the discernable peak splitting in $LiTi_2O_{4-\delta}$. Second, the valance of Ti in ideal $LiTi_2O_4$ is +3.5. If large numbers of oxygen vacancies exist in $LiTi_2O_{4-\delta}$, the $Ti^{3.5+}$ will transform to Ti^{3+}. In this condition, the electrons on t_{2g} band increase, and thereby the hoping possibility from Ti $2p$ to t_{2g} is reduced due to the Pauli Exclusion Principle. Consequently, oxygen vacancies will smear out the peaks of Ti $2p$ to t_{2g} in EELS.

Based on the EELS results, we can give a reasonable explanation for the suppression of the orbital-related state by filling oxygen vacancies. In general, the formation of the orbital order results from the band split near the Fermi level. As for $LiTi_2O_4$, crystal field splits Ti $3d$ bands to e_g and t_{2g} bands[33]. The oxygen vacancies in $LiTi_2O_{4-\delta}$ system, on the one hand, enhance the distortion of Ti-O octahedrons, on the other hand, dope electrons to enhance the electron correlations, which are beneficial to the formation of the orbital-related state. With the filling of oxygen vacancies, the valence of Ti increases and some of Ti sites become empty states, thereby weaken the orbital-related state.

Compared to the obviously suppressed orbital-related state, the T_{c0} of the $LiTi_2O_{4-\delta}$ thin films is quite stable at $P_{O2} < 5.4 \times 10^{-6}$ Torr. Actually, the O 2*p* bands are far below the Fermi level with weak *p*-*d* hybridizations[30,33]. Although the oxygen vacancies induce doping effect and influence on the splitting of Ti 3*d* bands by the crystal field, the density of states near Fermi surface may not change obviously, and thus the T_{c0} remains the same.

In conclusion, we studied the evolution from $LiTi_2O_{4-\delta}$ to $Li_4Ti_5O_{12}$ with increasing oxygen pressure during the thin film deposition. By transport and STEM measurements, we have disclosed that there are two processes happened during the evolution, *i.e*. the filling of oxygen vacancies and the forming of $Li_4Ti_5O_{12}$. The EELS results of the $LiTi_2O_{4-\delta}$ and $Li_4Ti_5O_{12}$ samples provide the evidence that the orbital-related state is suppressed by the filling of oxygen vacancies. The evolution of electronic states by adjusting the oxygen content gives an insight into the interaction between the orbital-related state and the superconductivity in $LiTi_2O_{4-\delta}$.

Methods

The (00*l*)-oriented $Li_{1+x}Ti_{2-x}O_{4-\delta}$ ($0 \leq \times \leq 1/3$) thin films are grown on (00 *l*) $MgAl_2O_4$ (MAO) substrates by PLD with a K_rF excimer laser ($\lambda = 248$ nm). Before the deposition, the MAO substrates are annealed at 1000 °C for 5 hours in the air[37,38] to obtain the smooth surface. The sintered $Li_4Ti_5O_{12}$ ceramic target is used to fabricate the films, with pulse frequency of 4 Hz, energy density of 1.5 J/cm^2, and deposition temperature of ~700 °C. The deposition rate is determined by measuring the thickness of ultra-thin films using X-ray reflectivity analysis. In this study, we fix the film thickness ~150 nm. After the deposition, all the thin films are quenched to the room temperature *in situ*.

X-ray diffraction (XRD) is employed to characterize the phase and crystalline quality of $Li_{1+x}Ti_{2-x}O_{4-\delta}$ ($0 \leq \times \leq 1/3$) thin films. The microstructure is detected by the spherical aberration-corrected scanning transmission electron microscopy techniques (Cs-STEM). The transport properties are measured by the Quantum Design Physical Property Measurement System (PPMS) with the temperature down to 2 K and magnetic field up to 9 T. Samples are etched into Hall bar by the UV lithography and Ar plasma etching technology for the measurement of the resistance properties.

References

1. Armitage, N. P., Fournier, P. & Greene, R. L. Progress and perspectives on electron-doped cuprates. *Rev. Mod. Phys.* **82**, 2421–2487 (2010).
2. Zhang, X. *et al*. Transport anomalies and quantum criticality in electron-doped cuprate superconductors. *Physica C* **525-526**, 18–43 (2016).
3. Kussmaul, A., Moodera, J. S., Tedrow, P. M. & Gupta, A. Improved laser-ablated thin films of NdCeCuO by use of N_2O. *Appl. Phys. Lett.* **61**, 2715–2717 (1992).
4. Lin, W. T. & Chen, Y. F. Oxygen pressure dependence of *in situ* growth of NdCeCuO thin films by laser ablation. *Appl. Phys. Lett.* **64**, 2157–2159 (1994).
5. Jiang, W. *et al*. Anomalous transport properties in superconducting $Nd_{1.85}Ce_{0.15}CuO_{4\pm\delta}$. *Phys. Rev. Lett.* **73**, 1291–1294 (1994).
6. Higgins, J. S., Dagan, Y., Barr, M. C., Weaver, B. D. & Greene, R. L. Role of oxygen in the electron-doped superconducting cuprates. *Phys. Rev. B* **73**, 104510 (2006).
7. Gauthier, J. *et al*. Different roles of cerium substitution and oxygen reduction in transport in $Pr_{2-x}Ce_xCuO_4$ thin films. *Phys. Rev. B* **75**, 024424 (2007).
8. Krockenberger, Y. *et al*. Emerging superconductivity hidden beneath charge-transfer insulators. *Sci. Rep.* **3**, 2235 (2013).
9. Cava, R. J. *et al*. Oxygen stoichiometry, superconductivity and normal-state properties of $YBa_2Cu_3O_{7-\delta}$. *Nature* **329**, 423–425 (1987).
10. Karpinski, J., Kaldis, E., Jilek, E., Rusiecki, S. & Bucher, B. Bulk synthesis of the 81-K superconductor $YBa_2Cu_4O_8$ at high oxygen pressure. *Nature* **336**, 660–662 (1988).
11. Chaud, X. *et al*. Flux mapping at 77 K and local measurement at lower temperature of thin-wall YBaCuO single-domain samples oxygenated under high pressure. *Physica C* **469**, 1200–1206 (2009).
12. Schooley, J. F., Hosler, W. R. & Cohen, M. L. Superconductivity in semiconducting $SrTiO_3$. *Phys. Rev. Lett.* **12**, 474–475 (1964).
13. Jourdan, M., Blumer, N. & Adrian, H. Superconductivity of $SrTiO_{3-\delta}$. *Eur. Phys. J. B* **33**, 25–30 (2003).
14. Zhang, C. *et al*. Enhanced superconductivity in TiO epitaxial thin films. *npj Quant. Mater.* **2**, 1–5 (2017).
15. Reed, T. B., Banus, M. D., Sjöstrand, M. & Keesom, P. H. Superconductivity in cubic and monoclinic "TiO". *J. Appl. Phys.* **43**, 2478–2479 (1972).
16. Kang, H. J. *et al*. Electronically competing phases and their magnetic field dependence in electron-doped nonsuperconducting and superconducting $Pr_{0.88}LaCe_{0.12}CuO_{4\pm\delta}$. *Phys. Rev. B* **71**, 214512 (2005).
17. Chang, J. *et al*. Direct observation of competition between superconductivity and charge density wave order in $YBa_2Cu_3O_{6.67}$. *Nat. Phys.* **8**, 871–876 (2012).
18. Wuyts, B., Moshchalkov, V. V. & Bruynseraede, Y. Resistivity and Hall effect of metallic oxygen-deficient $YBa_2Cu_3O_x$ films in the normal state. *Phys. Rev. B* **53**, 9418–9432 (1996).
19. Allgeier, C. & Schilling, J. S. Correlation between the magnitude of the superconducting transition temperature and the normal-atate magnetic susceptibility in $Bi_2Sr_2CaCu_2O_{8+y}$ and $Tl_2Ba_2CuO_{6+y}$ as a function of oxygen content. *Physica C* **168**, 499–505 (1990).
20. Tanabe, K., Kubo, S., Teherani, F. H., Asano, H. & Suzuki, M. Effects of photoinduced hole doping on normal-state and superconducting transport in oxygen-deficient $YBa_2Cu_3O_y$. *Phys. Rev. Lett* **72**, 1537–1540 (1994).
21. Moshopoulou, E. G. Superconductivity in the Spinel Compound $LiTi_2O_4$. *J. Am. Ceram. Soc.* **82**, 3317–3320 (1999).
22. Johnston, D. C., Prakash, H., Zachariasen, W. H. & Viswanathan R. High Temperature Superconductivity In The Li-Ti-O Ternary System. *Mat. Res. Bull.* **8**, 777–784 (1973).
23. Sun, C. P. *et al*. Magnetic field dependence of low-temperature specific heat of the spinel oxide superconductor $LiTi_2O_4$. *Phys. Rev. B* **70**, 054519 (2004).
24. Tang, L. *et al*. Electrical resistivity and Andreev reflection spectroscopy of the superconducting oxide spinel $LiTi_2O_4$. *Phys. Rev. B* **73**, 184521 (2006).
25. Johnston, D. C. Superconducting and normal state properties of $Li_{1+x}Ti_{2-x}O_4$ spinel compounds. I. preparation, crystallography, superconducting properties, electrical resistivity, dielectric behavior, and magnetic susceptibility. *J. Low. Temp. Phys.* **25**, 145–175 (1976).
26. Chen, C. L. *et al*. Role of 3d electrons in the rapid suppression of superconductivity in the dilute V doped spinel superconductor $LiTi_2O_4$. *Supercond. Sci. Technol.* **24**, 115007 (2011).
27. Tunstall, D. P. *et al*. Titanium nuclear magnetic resonance in metallic superconducting lithium titanate and its lithium-substituted derivatives $Li_{1+x}Ti_{2-x}O_4$ ($0 < \times < 0.10$). *Phys. Rev. B* **50**, 16541–16549 (1994).
28. Jin, K. *et al*. Anomalous magnetoresistance in the spinel superconductor $LiTi_2O_4$. *Nat. Commun.* **6**, 7183 (2015).

29. Kumatani, A. *et al.* Growth processes of lithium titanate thin films deposited by using pulsed laser deposition. *Appl. Phys. Lett.* **101**, 123103 (2012).
30. Massidda, S., Yu, J. & Freeman, A. J. Electronic structure and properties of superconducting $LiTi_2O_4$. *Phys. Rev. B* **38**, 11352–11357 (1988).
31. He, G. *et al.* Anisotropic electron-phonon coupling in the spinel oxide superconductor $LiTi_2O_4$. *Phys. Rev. B* **95**, 054510 (2017).
32. Lu, X. *et al.* Lithium storage in $Li_4Ti_5O_{12}$ spinel: the full static picture from electron microscopy. *Adv. Mater.* **24**, 3233–3238 (2012).
33. Satpathy, S. & Martin, R. M. Electronic structure of the superconducting oxide spinel $LiTi_2O_4$. *Phys. Rev. B* **36**, 7269–7272 (1987).
34. Bulgadaev, S. A. & Kusmartsev, F. V. Large linear magnetoresistivity in strongly inhomogeneous planar and layered systems. *Phys. Lett. A* **342**, 188–195 (2005).
35. Hewett, T. H. & Kusmartsev, F. V. Geometrically enhanced extraordinary magnetoresistance in semiconductor-metal hybrids. *Phys. Rev. B* **82**, 212404 (2010).
36. Liu, Y. X. *et al.* The first-principles study for the novel optical properties of $LiTi_2O_4$, $Li_4Ti_5O_{12}$, $Li_2Ti_2O_4$ and $Li_7Ti_5O_{12}$. *Chem. Phys. Lett.* **677**, 114–119 (2017).
37. Maruyama, S. *et al.* Reversible electrochemical modulation of the superconducting transition temperature of $LiTi_2O_4$ ultrathin films by ionic liquid gating. *Appl. Phys. Lett.* **107**, 142602 (2015).
38. Zhao, M. L. *et al.* Investigation of the optical properties of $LiTi_2O_4$ and $Li_4Ti_5O_{12}$ spinel films by spectroscopic ellipsometry. *Optic. Mater. Express* **6**, 3366 (2016).

Acknowledgements

We thank K. Liu for fruitful discussions and L. H. Yang for technique support. This work was supported by the National Key Basic Research Program of China (2015CB921000, 2016YFA0300301, 2017YFA0303003, 2017YFA0302902), the National Natural Science Foundation of China (11674374, 11474338), the Beijing Municipal Science and Technology Project (Z161100002116011, D161100002416003, D161100002416001), the Key Research Program of the Chinese Academy of Sciences, (Grant NO. XDPB01), the Key Research Program of Frontier Sciences, CAS (QYZDB-SSW-SLH001, QYZDB-SSW-SLH008), the Open Research Foundation of Wuhan National High Magnetic Field Center (PHMFF2015008), and the Strategic Priority Research Program of the CAS (XDB07020100).

Author Contributions

Y.J. and J.Y. designed and performed electrical transport experiments; G.H. and Y.J. analyzed data and wrote the main manuscript text; Y.J., W.H., H.Y. and Z.L. prepared the samples and performed structural characterizations; L.G., Z.Y. and J.S. did the Cs-corrected STEM experiments; G.H., Y.J., W.H., H.Y., Q.Z., B.Z., H.L. and K.J. contributed to the discussions and writing; K.J. supervised the project.

Additional Information

Competing Interests: The authors declare no competing interests.

Publisher's note: Springer Nature remains neutral with regard to jurisdictional claims in published maps and institutional affiliations.